



Power Electronic Systems
Laboratory

© 2013 IEEE

Proceedings of the 28th Applied Power Electronics Conference and Exposition (APEC 2013), Long Beach, California, USA,
March 17-21, 2013

Optimized Magnetic Design for Inductive Power Transfer Coils

R. Bosshard,
J. Mühlethaler,
J. W. Kolar,
I. Stevanovic

This material is published in order to provide access to research results of the Power Electronic Systems Laboratory / D-ITET / ETH Zurich. Internal or personal use of this material is permitted. However, permission to reprint/republish this material for advertising or promotional purposes or for creating new collective works for resale or redistribution must be obtained from the copyright holder. By choosing to view this document, you agree to all provisions of the copyright laws protecting it.



Eidgenössische Technische Hochschule Zürich
Swiss Federal Institute of Technology Zurich

Optimized Magnetic Design for Inductive Power Transfer Coils

R. Bosshard*, J. Mühlethaler*, J. W. Kolar*, and I. Stevanović†

*Power Electronic Systems Laboratory, ETH Zürich, Switzerland, Email: bosshard@lem.ee.ethz.ch

†ABB Switzerland Ltd., Corporate Research, 5405 Baden-Dättwil, Switzerland

Abstract—Inductive Power Transfer (IPT) is well-established for applications with biomedical implants and radio-frequency identification systems. Recently, also systems for the charging of the batteries of consumer electronic devices and of electric and hybrid electric vehicles have been developed. The efficiency η of the power transfer of IPT systems is given by the inductor quality factor Q and the magnetic coupling k of the transmission coils. In this paper, the influence of the transmission frequency on the inductor quality factor and the efficiency is analyzed taking also the admissible field emissions as limited by standards into account. Aspects of an optimization of the magnetic design with respect to a high magnetic coupling and a high quality factor are discussed for IPT at any power level. It is shown that the magnetic coupling mainly depends on the area enclosed by the coils and that their exact shape has only a minor influence. The results are verified with an experimental prototype.

I. INTRODUCTION

Inductive Power Transfer (IPT) is well-established as a technique to deliver small amounts of energy to remote devices. It has been used for the supply of microelectronic implants such as neuromuscular stimulators, visual prostheses, and cortical implants [1]–[4] or even to deliver power to an artificial heart [5], [6]. In biomedical applications, IPT offers the possibility to reduce infections due to the elimination of the previously required wired connections for the power and data transmission that were running through the patient’s skin.

Similarly, Radio-Frequency Identification (RFID) is a mature technology that makes use of IPT to gather information from identification tags or remote sensors [7], [8]. Lately, also consumer electronics applications have emerged, for instance in the form of charging pads for mobile phones [9], and IPT has been proposed for the charging of the traction batteries of Electric and Hybrid Electric Vehicles (EV/HEV) in recent publications [10]–[15]. Domestic induction cooking shall be mentioned as a related application [16]–[18], where similar coil geometries and power electronic circuits are used at comparable power levels.

Among the different IPT applications, similar performance criteria exist for all power levels. For instance in biomedical applications, the amount of available space for an implant in the patient’s body is limited. Similar limitations also exist with EV/HEV applications. There, the space for the receiver coil on the underfloor of the vehicle is typically specified by the vehicle manufacturer. Hence, the size of the inductor coils and the power electronics is limited, which implies the requirement for a high power density of the transmission coils. Additionally, the transmission efficiency should be as high as possible to deliver the required output power with a low power loss and, in many applications, only a small resulting increase of the operating temperature of the devices [13]. For an optimal performance, the alignment of the transmission coils is of high importance. In a practical system a misalignment of the coils is likely if no additional positioning aids are used. Therefore, an IPT system must also be capable of operating under these conditions. Another design constraint arises from the limitations on the leakage flux in the vicinity of the coils. In order to prevent health risks

resulting from induced electric fields in human tissue, specifically in the brain and the retina, the emitted leakage fields are limited by standards [19], [20].

The magnetic design of the transmission coils is of key importance in order to satisfy these requirements. Even though a large number of magnetic structures for IPT inductors have been proposed in literature, no systematic way for optimizing the magnetic design of the IPT coils was presented so far. Therefore, this paper aims to provide a set of design guidelines for the magnetic optimization, namely the used operating frequency, the geometric design of the coils and the use of core materials.

It was shown in [21], [22] that a Figure-of-Merit $FOM = kQ$ given by the product of the magnetic coupling k and the inductor quality factor Q limits the maximum efficiency of the power transmission to approximately $\eta_{\max} \approx 1 - 2/(kQ)$. Hence, these two parameters should be maximized in the design of the coils in order to achieve a high efficiency.

In order to maximize the quality factor $Q \approx \omega_0 L/R_{ac}$ of the transmission coils, a high operating frequency would be desirable, because the quality factor increases with increasing frequency despite the increasing ac resistance of the windings. Fig. 1 shows a comparison of the power levels and the transmission frequencies used in practical IPT applications found in literature. A trend to higher transmission frequencies exists at lower power levels. Thanks to the higher availability of fast-switching semiconductor devices at these power levels, the practically feasible switching frequencies reach up into the MHz-range. The increased operating frequency leads to smaller coil sizes for a given air gap, since the reduction in magnetic coupling k can to some extent be compensated by the higher coil quality factor Q . The selection of the operating frequency, however, is also influenced by the norms regulating the leakage flux emissions in the vicinity of the coils.

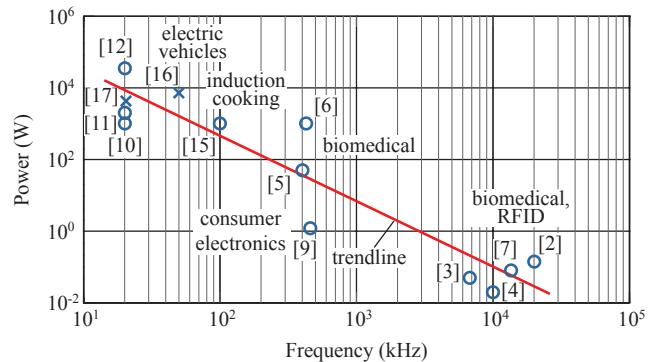


Fig. 1. Comparison of the power levels and the used transmission frequency of IPT systems in biomedical, RFID, consumer electronics, and EV/HEV applications. Inductive cooking applications are marked with a cross.

How the switching frequency should be chosen taking all aspects into consideration is analyzed in more detail in Section II. A study of the influence of the inductor geometry on the magnetic coupling k is presented in Section III. Later, in Section IV, the question of an optimal selection and placement of the windings on the coil area is addressed. The size of the transmitter coil can still be adjusted, because in typical IPT applications only the size of the receiver coil is limited. The relative size of the receiver and transmitter coils are commonly believed to be equal for an optimal coil design. However, this assumption can be disproved with a numerical calculation. From the obtained results, suggestions for an optimal selection of the transmitter coil size for a given receiver coil size and air gap width are derived.

Especially at higher power levels, where the thermal constraints become more restrictive, the use of magnetic materials for guiding the magnetic flux is proposed to improve the coupling of the coils. Section V provides an insight into the advantages and disadvantages of different core structures for IPT systems.

In order to support the obtained theoretical results, 2D and 3D Finite Element (FE) simulations are used throughout this paper. Additionally, a prototype inductor was constructed and an experimental verification of the results is presented in Section VI.

II. SELECTION OF THE TRANSMISSION FREQUENCY

Independent of their power level, IPT systems suffer from a low magnetic coupling of typically less than 30% due to the high leakage inductance of the coils caused by the large air gap between the transmitter and the receiver. It was shown in previous publications that this imposes an inherent limitation on the efficiency η of the power transfer [22]. The efficiency can be increased if a resonant compensation of the receiver with either a parallel or a series connected compensation capacitor is used. This is shown in Fig. 2(a)-(b). Another compensation capacitor is typically added at the primary side in order to reduce the reactive power that needs to be delivered by the supply. The result is a highly selective bandpass characteristic of the input impedance of the circuit. Therefore, if both sides of the resonant circuit are tuned to the same resonance frequency f_0 , the currents in the transmission coils are approximately sinusoidal.

Under this assumption, it can be shown that for both compensation topologies, the maximum achievable transfer efficiency is given by [22]

$$\eta_{\max} = \frac{(kQ)^2}{\left(1 + \sqrt{1 + (kQ)^2}\right)^2}, \quad (1)$$

where k is the magnetic coupling between the coils and Q is the inductor quality factor. The inductor quality factor of the transmission coils is defined by the geometric average of the two individual coil quality factors $Q = \sqrt{Q_1 Q_2}$, which are given by [23]

$$Q_i = \frac{\omega_0 W_{L_i}}{P_{\text{loss},i}} \approx \frac{\omega_0 L_i}{R_{\text{ac},i}}, \quad (2)$$

where $\omega_0 = 2\pi f_0$ is the angular transmission frequency, W_{L_i} and $P_{\text{loss},i}$ are the stored energy and the power loss in inductor $i = 1, 2$ respectively, L_i is the inductance of the respective coil, and $R_{\text{ac},i}$ is its ac resistance at the operating frequency.

According to (1), the maximum transfer efficiency η_{\max} is fully defined by the $FOM = kQ$. Note that for high values of the FOM , (1) is approximately equal to $\eta_{\max} \approx 1 - 2/(kQ)$ [9], [13]. It follows that in order to maximize the efficiency of the power transfer, the FOM of IPT coils must be as high as possible.

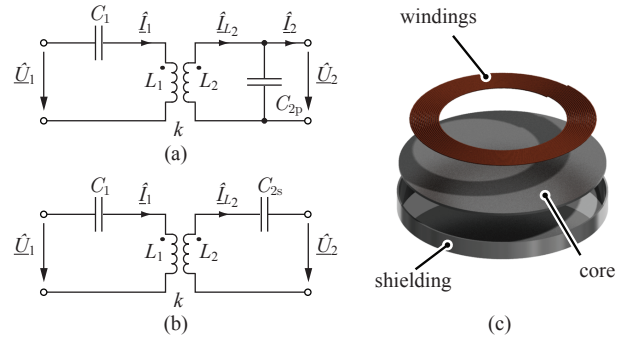


Fig. 2. Resonant compensation topologies: (a) parallel compensated receiver; (b) series compensated receiver. Drawing of a typical IPT inductor (c).

From (1) and (2), it is clear that the transmission frequency has a high influence on the efficiency of the system. Therefore, this section continues with an analysis of the frequency dependency of the loss components present in a typical IPT inductor. In the second part, their impact on the transmission efficiency is discussed. In the last part, the influence of the leakage flux limitations on the frequency selection and on the transmitted power is investigated.

A. Inductor Loss Components

In Fig. 2(c), a schematic drawing of an IPT inductor that includes copper windings, a core (e.g. ferrite), and shielding materials (e.g. aluminum) is shown. The total power loss in such an inductor can be approximated by

$$P_{\text{loss}} = P_w + P_c + P_s, \quad (3)$$

where P_w represents the conduction losses in the windings including the losses due to the skin and the proximity effect. The core losses are represented by P_c , and P_s stands for the eddy current losses in the shielding materials of the inductor, if such components are part of the inductor design.

The skin and the proximity losses can be calculated from the amplitude of the winding current \hat{I} , the external magnetic field that penetrates the windings, the operating frequency, and the parameters of the litz wire used for the construction [24]. It can be shown that the skin effect losses increase with a proportionality between linear and quadratic to the operating frequency for low frequencies, whereas for higher frequencies they tend to a proportionality to the square root of the operating frequency.

The losses due to the internal and the external proximity effect show a proportionality to the square of the operating frequency up to the point where the skin depth reaches the dimension of one strand diameter. Above, the increase of the proximity losses also follows the square root of the operating frequency. As a result, the total winding losses increase with a proportionality of less than the square of the operating frequency for low frequencies and with its square root at higher frequencies

$$P_w \propto \hat{I}^2 \cdot \begin{cases} f_0^{<2}, & \text{for low } f_0 \\ \sqrt{f_0}, & \text{for high } f_0. \end{cases} \quad (4)$$

Due to the sinusoidal excitation, the losses per unit volume of the core P'_c can be calculated using the Steinmetz equation

$$P'_c = \kappa f_0^\alpha \hat{B}^\beta, \quad (5)$$

where κ , α , and β are the Steinmetz coefficients of the core material.

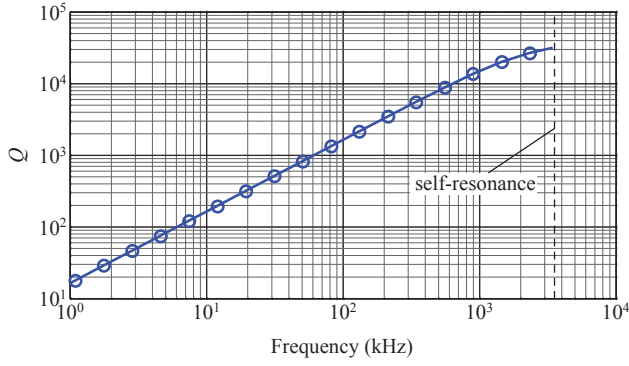


Fig. 3. Simulated quality factor of the prototype coil used in Section VI. The self resonance was determined to be 3.3 MHz, which for this case is the optimal operating point.

The eddy current losses in the shielding material can be estimated from the field strength penetrating the shielding material and the skin depth of the material at the operating frequency. Assuming that the magnetic field strength is proportional to the current in the winding of the inductor and that the skin depth is smaller than the dimensions of the shielding material, one can show that the resulting eddy current losses are proportional to the square of the current amplitude and to the square root of the operating frequency

$$P_s \propto \sqrt{f_0} \cdot \hat{I}^2. \quad (6)$$

B. Transmission Efficiency

If the transmission frequency is increased, the magnetizing current \hat{I}_h is reduced according to

$$\hat{I}_h \propto \frac{1}{f_0}. \quad (7)$$

Therefore, also the currents in the windings decrease if the transferred power is kept constant. Since the core losses are proportional to \hat{B}^β and $\beta > \alpha$ for typical core materials, they decrease with increasing operating frequency, because the magnetic flux density in the core is proportional to the current in the windings. As shown above, all other loss components are proportional to the square of the current amplitude and exhibit a proportionality lower than square to the operating frequency, which implies that they also decrease with increasing frequency. As soon as the magnetizing current \hat{I}_h becomes comparable to the active part of the winding current that is needed for the transmission of the power, the losses are no longer dominated by \hat{I}_h . Above this point, a further increase of the transmission frequency will lead to increasing losses and the efficiency will decrease. Therefore, an increase of the operating frequency leads to decreasing losses and an increase of the coil quality factor up to a certain optimal value which remains to be determined. If the ac losses in the windings are low, this point lies above the self-resonant frequency, which would then be the optimal operating point.

Simulation results obtained with the 2D FE tool FEMM¹ for the quality factor of the prototype coil used in Section VI are shown in Fig. 3 to verify the considerations above. It can be seen that the quality factor increases up to the self-resonance frequency of 3.3 MHz, which in this case would be the optimal operating point. Note that the capacitive effects were not included into the simulation.

¹Available at www.femm.info (12.11.2012)

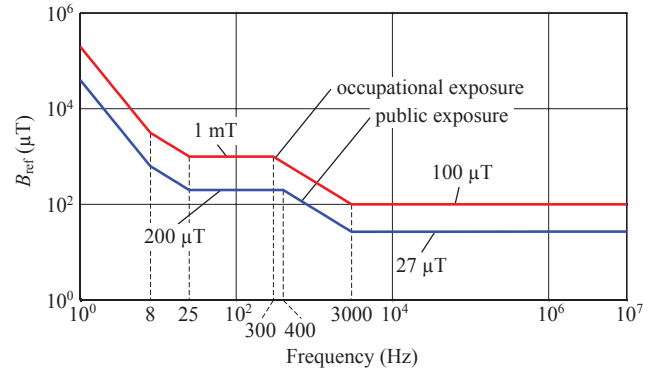


Fig. 4. Reference levels for the magnetic flux density for the general public and occupational exposure as published by the ICNIRP in 2010 [19].

Therefore, the indicated self-resonance frequency was obtained from an impedance measurement on the experimental prototype.

C. Transmitted Power

The transmitted power in a series compensated IPT system (cf. Fig. 2(b)) is proportional to the operating frequency f_0 and the flux linkage $L_h \hat{I}_h$

$$P_\delta \propto U_{\text{ind}}^2 \propto (f_0 L_h \hat{I}_h)^2. \quad (8)$$

Given that the magnetic flux density in the air gap \hat{B}_h is proportional to the flux linkage, i.e. the coil design is kept the same, (8) can be expressed as

$$P_\delta \propto (f_0 \hat{B}_h)^2, \quad (9)$$

which illustrates that for a given coil design, a higher power can be transmitted either by using a higher operating frequency or by increasing the flux density in the air gap.

Assuming that the flux density at the point where the standards regulating the leakage flux emissions should be respected is proportional to the magnetizing flux density \hat{B}_h , which is likely to be the case with any IPT inductor, the maximum transmittable power $P_{\delta, \text{max}}$ at a given frequency is related to the reference value by

$$P_{\delta, \text{max}} \propto (f_0 B_{\text{ref}})^2. \quad (10)$$

The maximum transmittable power is reached if the flux density lies just below the limit value defined by the standards. The guidelines published by the International Commission on Non-Ionizing Radiation Protection (ICNIRP) are commonly used as reference levels for the leakage flux in the vicinity of IPT coils. Fig. 4 shows the 2010 reference values for the magnetic flux density as a function of the operating frequency [19].

If the maximum flux density for a given inductor is reached, the transmitted power can only be increased further if a higher operating frequency at a constant flux linkage $L_h \hat{I}_h$ is used. However, this requires that the voltage levels at the input and the output terminals are increased. In practice, this is only possible if series connected capacitors are used for the resonant compensation of the large coil voltages at the transmitter as well as on the receiver side (cf. Fig. 2(b)). With a parallel connected compensation capacitor, the high voltage would be directly visible at the load (cf. Fig. 2(a)) and also at the supply, if a parallel compensation is used also on the transmitter side. However, the choice of the compensation topology is also influenced by the power level and the physical size of the

system [13], [21]. To reach the maximum efficiency η_{\max} with a series compensation of the receiver coil, large inductors are required which could be undesirable. Therefore, an increase of the transmission frequency at a constant flux linkage $L_h \hat{I}_h$ may not be possible.

Additionally, note that a frequency increase only allows a higher power transmission in the range from 25 to 300 Hz for the occupational exposure reference level or to 400 Hz for the general public exposure reference level, and between 3 kHz and 10 MHz, where the respective reference value is constant. In the range from 300 Hz or 400 Hz to 3 kHz, however, the reference value is decreasing with $B_{\text{ref}} \propto 1/f_0$. In this region, a higher frequency requires a reduction of the magnetic flux density in the air gap. Therefore, the transmitted power must remain constant

$$P_{\delta, \max} \propto \left(f_0 \cdot \frac{1}{f_0} \right)^2 \equiv 1 \quad (11)$$

if the frequency is increased.

D. Discussion

In order to maximize the efficiency of an IPT system, the quality factor should be maximized. According to the considerations above, the operating frequency can be used for that purpose as was done for instance in [25]. However, the quality factor only increases up to a certain maximum value. This frequency would then be the optimal operating point from the point of view of the transmission efficiency. If this operating point lies above the self-resonance frequency of the coils, i.e. if the ac losses in the windings are low, the self-resonant frequency would be the optimal operating point. This was proposed for instance in [26].

However, the losses in the power electronic circuits were not discussed in these considerations. Even if soft-switching control methods are used to reduce the switching losses at the higher frequencies [14], for instance the losses in conventional gate drivers will still increase for a higher switching frequency. Additionally, if IGBTs are used for the switches of the supply inverter, also high switching losses would occur [27]. An optimum operating frequency could be determined if these factors were also included into the calculation. In conclusion, this shows that the power electronics are an important limiting part of an IPT system and must, therefore, be considered in an overall system optimization.

III. OUTER SHAPE OF THE INDUCTOR

Apart from the quality factor of the inductor, the magnetic coupling k defines the efficiency of the power transfer. For its maximization, an optimized magnetic design of the inductor is of high importance.

Typical shapes of IPT inductors include circular, square, and rectangular structures (cf. Fig. 5(a)-(c)). Additionally, a splitting of the available area into two electrically parallel connected segments as shown in Fig. 5(d) was proposed in [11]. However, it is not clear if and by how much the coupling can be improved by either of these geometries. Therefore, in this section the performance in terms of the magnetic coupling of different coil geometries is analyzed.

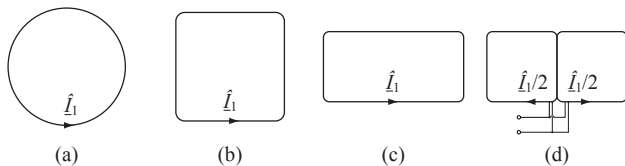


Fig. 5. Schematic drawing of the simulated inductor shapes: (a) circular coil; (b) square coil; (c) rectangular coil; (d) segmented coil.

TABLE I
GEOMETRY PARAMETERS OF THE FE MODELS

Area = 314.2 cm ² , $d_w = 1$ mm, $N_{1,2} = 1$, $\delta = 70$ mm				
Value	Circular	Square	Rectangular	Segmented
Radius	100 mm	-	-	-
Length	-	177.3 mm	250.7 mm	250.7 mm
Width	-	177.3 mm	125.3 mm	125.3 mm
Area = 628.3 cm ² , $d_w = 1$ mm, $N_{1,2} = 1$, $\delta = 70$ mm				
Value	Circular	Square	Rectangular	Segmented
Radius	141.4 mm	-	-	-
Length	-	250.6 mm	354.5 mm	354.5 mm
Width	-	250.6 mm	177.3 mm	177.3 mm
Area = 1256.6 cm ² , $d_w = 1$ mm, $N_{1,2} = 1$, $\delta = 70$ mm				
Value	Circular	Square	Rectangular	Segmented
Radius	200 mm	-	-	-
Length	-	354.5 mm	501.3 mm	501.3 mm
Width	-	354.5 mm	250.7 mm	250.7 mm

A. Simulated Inductor Shapes

In order to compare the performance of the different coil shapes, the 3D FE tool COMSOL² was used. Models of a circular, a square, and a rectangular coil geometry, as well as a segmented geometry, similar to what is presented in [11], but without the ferrite cores, were built in three different sizes to compare their magnetic coupling coefficients. The geometry parameters of the models are shown in Table I.

For all models, a small conductor diameter of $d_w = 1$ mm was used and the number of turns were set to $N_1 = N_2 = 1$, i.e. the winding was concentrated at the outer edge of the coil, in order to minimize any effects resulting from a finite size of the winding. The air gap was set to $\delta = 70$ mm. The radius of the circular coil was set to $R = 100$ mm, 141.4 mm, and 200 mm. The three resulting coil areas were taken as a reference for the other models, which were then designed to have the same area. The rectangular and the segmented coil were designed with a width to length ratio of 1/2.

With the FE tool, the magnetic flux density produced by a current in the transmitter coil was calculated. Next, the flux linkage of the two coils $\hat{\psi}_{12}$ was determined using a surface integration on the area A_2 enclosed by the receiver coil

$$\hat{\psi}_{12} = \iint_{A_2} \vec{B} \cdot d\vec{A}. \quad (12)$$

The self-inductance L_1 of the primary coil was calculated from the total magnetic energy $W_L = \frac{1}{2} L_1 \hat{I}^2$. In the case of equal primary and secondary self-inductances $L_2 = L_1$, this leads to the magnetic coupling coefficient

$$k = \frac{L_h}{\sqrt{L_1 L_2}} = \frac{\hat{\psi}_{12}}{\hat{I}} \cdot \frac{\hat{I}^2}{2W_L} = \frac{\hat{\psi}_{12} \hat{I}}{2W_L}. \quad (13)$$

A large simulation space and a fine mesh were used to minimize the influence of boundary effects and to maximize computation accuracy.

B. Comparison of the Results

The results of the simulations of the four coil shapes are shown in Fig. 6. The comparison shows that for a given size of the inductor area, the square coil and the rectangular coil achieve approximately the same magnetic coupling k . The magnetic coupling obtained with

²Available at www.comsol.com (12.11.2012)

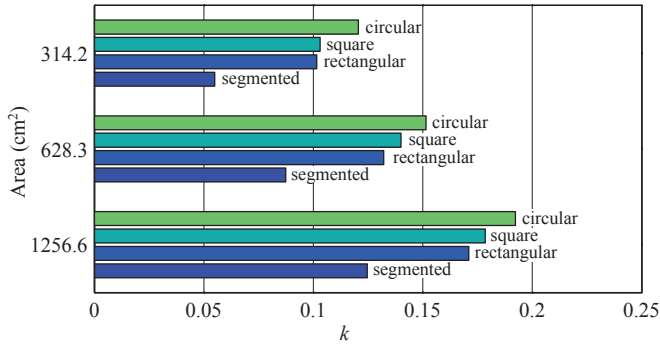


Fig. 6. Comparison of the results of the 3D FE simulations for the magnetic coupling k of the four inductor shapes shown in Fig. 5.

a circular coil of the same area is somewhat higher than that of the square and the rectangular coil. Presumably, this can be explained by the distortion of the field distribution around the corners of those shapes. With good accuracy, it can be concluded from these results that the parameter that mainly influences the magnetic coupling is the area enclosed by the inductor. The exact shape of the coil has only a minor influence.

Additionally, the results show that the segmented coil achieves a magnetic coupling that approximately corresponds to that of a rectangular coil with only half the size. This can be explained with the example of two parallel connected transformers: if two equal transformers are connected in parallel at their primary and secondary terminals, the self-inductance of the combined device is half of that of a single transformer. The same holds for the mutual inductance. Therefore, the parallel connected transformers have the same magnetic coupling than a single transformer. In the case of the segmented coil, each segment of the primary inductor together with the corresponding segment of the secondary inductor can be considered a separate transformer, if the cross-coupling between the two transformers is considered to be small. Then it is clear that the coupling of the complete inductor is approximately the same as that of a single pair of segments, which in turn corresponds to that of a rectangular coil with half the size.

In most IPT applications, the size of the receiver coil is limited. For biomedical systems, a small size of the implanted receiver is desired to minimize the space that is required for its placement within the patient's body. In applications with EV/HEV, a similar boundary condition exists: the space that is available at the underfloor of a vehicle is typically limited and relatively small when compared to the air gap. Additionally, for this case often a rectangular area is specified. According to the results presented in this section, the best option under these conditions is to fully utilize the available area for the receiver and keep the provided area shape.

IV. UTILIZATION OF THE INDUCTOR AREA

It was shown in the previous section, that the exact shape of the coils is less important than their size. Therefore, a set of circular spiral coils is used for the analysis presented in this section. This allows to use an exact calculation instead of FE simulations, which simplifies the analysis significantly. The next step after the selection of an inductor shape is the design and the placement of the windings. In the following, the influence of each of the remaining design parameters as shown in Fig. 7 on the magnetic coupling k of the coils is studied.

A. Calculation Method

For the calculation of the mutual inductance between two spiral coils without core materials, semi-analytical equations³ exist [28]. These equations can also be used for the calculation of the self-inductance, if they are adapted accordingly. Note that the equations used in [28] are exact, if the numerical parts are evaluated with sufficient accuracy. A deviation of less than 5% from the inductance values obtained from FE simulations was observed.

In order to determine the influence of each of the design parameters outlined in Fig. 7, a series of calculations was conducted where the parameters were varied one-by-one. For this process, the outer receiver coil radius was assumed to be fixed to $R_{a,2} = 100$ mm. All results are shown for the three different air gaps $\delta = 25, 75,$ and 150 mm. The number of turns of the receiver was set to $N_2 = 15$. The conductor diameter and the separation of the windings were adjusted as described below.

B. Influence of the Conductor Diameter

In a first step, the diameter of the conductors in both coils was varied between 0.5 mm and 5 mm. The outer radius of the transmitter coil and the primary number of turns were constantly maintained at $R_{a,1} = 100$ mm and $N_1 = 15$, equal to the parameters of the receiver. Also the inner radius was kept equal and constant at $R_i = 11.5$ mm for both coils. This means that for a smaller conductor diameter, the windings are separated more than for a large conductor diameter.

The result of the calculation of the magnetic coupling k at the three different values of the air gap δ is shown in Fig. 8(a). Only a low variation of the coupling results from the variation of d_w and s_w . Apparently, the conductor diameter and the separation of the windings have no significant influence on k .

C. Influence of the Number of Turns

A similar study can also be conducted for a variable number of turns. The inner and outer radii of the coils were kept constant at the same values as before. This time, the separation of the windings was kept constant at $s_w = 1$ mm. The secondary number of turns was also kept constant at $N_2 = 15$. The primary number of turns N_1 was varied from 5 to 30 turns, while the conductor diameter was adjusted such that the windings were equally distributed between the inner and the outer coil radius.

The calculated coupling coefficient is shown in Fig. 8(b). Because the secondary number of turns was not varied in this calculation,

³Due to the complexity of these equations, they are not repeated here for the sake of clarity. However, their application is straight forward from the cited publication.

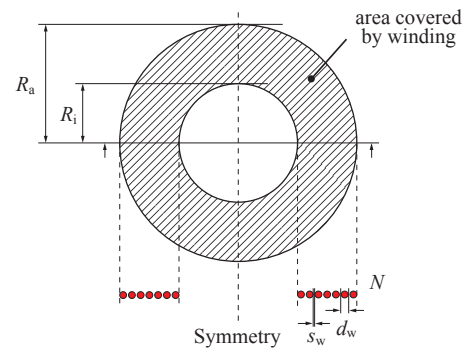


Fig. 7. The design parameters of a circular spiral coils are the winding diameter d_w , the separation of the windings s_w , the number of turns N , and the inner and outer coil radius R_i, R_a respectively.

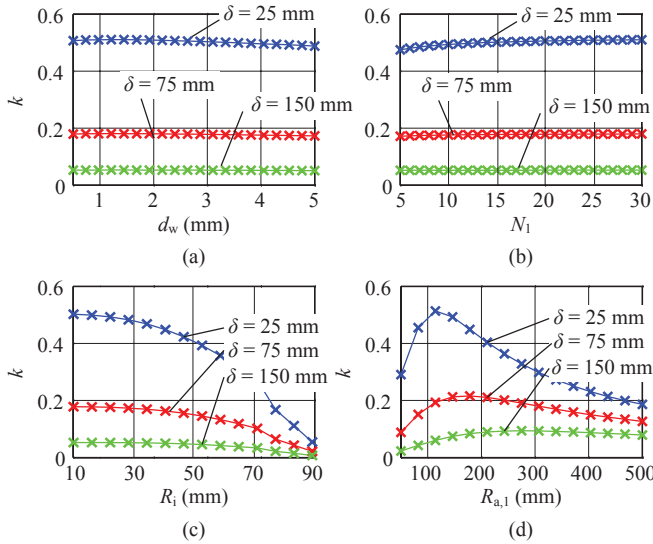


Fig. 8. Calculated coupling coefficient k for the air gaps $\delta = 25, 75,$ and 150 mm: (a) variation of the conductor diameter in both coils; (b) variation of the primary number of turns; (c) variation of both inner coil radii; (d) variation of the outer radius of the transmitter coil.

the ratio N_1/N_2 was not constant. Except for the smallest air gap and for the lowest N_1 values, where the separation of the windings is largest, also the primary number of turns and the ratio N_1/N_2 have no significant impact on the coupling coefficient. This result is intuitively clear considering $k = L_h/\sqrt{L_1 L_2}$, where the number of turns cancels out for conventional transformers.

D. Influence of the Inner Coil Radius

In the next step, the inner radii of the two coils were varied equally from 10 mm to 90 mm ($R_{i,1} = R_{i,2}$). The outer coil radii were again kept constant at 100 mm. This time, also the winding separation and the conductor thickness were kept constant at $s_w = 1$ mm and $d_w = 4.9$ mm respectively. The primary and the secondary number of turns were adjusted to the variable inner radius.

The resulting coupling coefficients are shown in Fig. 8(c). Clearly, the inner coil radius has a significant influence on the magnetic coupling of the two coils. The magnetic coupling increases with decreasing inner radius of the coils, which was also observed in [1]. Accordingly, the inner radius of the spiral coil should be made as small as possible to achieve a high magnetic coupling.

E. Influence of the Outer Coil Radius

In a last series of calculations, the magnetic coupling was determined for a variable outer radius of the transmitter coil for a fixed size of the receiver coil $R_{a,2} = 100$ mm. As a conclusion from the previous step, the inner radii of both coils were set to zero, which implies $N_2 = 16$ for these calculations. The conductor diameter and the winding separation were held constant at $s_w = 1$ mm and $d_w = 4.9$ mm, which means that the increased outer radius of the transmitter coil was obtained by adding more primary windings.

The calculated magnetic coupling values are shown in Fig. 8(d). A maximum of the coupling coefficient can be observed at a certain outer radius of the transmitter coil, which is larger than that of the receiver coil. Contrary to a common assumption, for larger air gaps the maximum of the magnetic coupling k cannot be reached with coils of equal size. Fig. 9 shows the contour lines of the magnetic coupling k for different air gaps and transmitter coil radii for a given

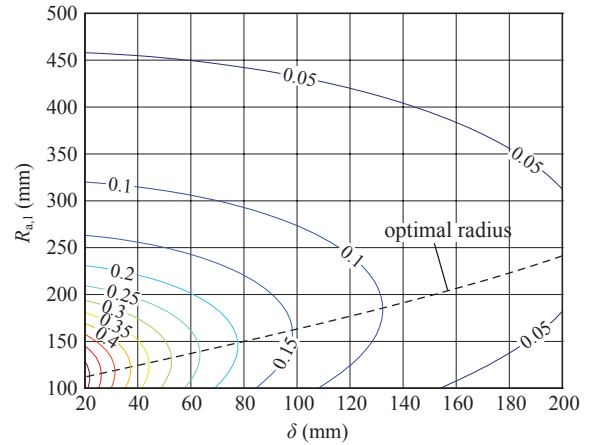


Fig. 9. Contour lines of the magnetic coupling obtained for different values of the air gap δ and the transmitter coil radius $R_{a,1}$ for a given receiver coil with $R_{a,2} = 100$ mm and $N_1 = N_2 = 15$ with $d_w = 4.9$ mm, $s_w = 1$ mm.

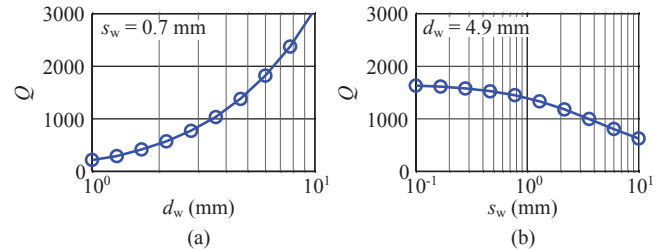


Fig. 10. Simulated quality factor at 100 kHz: (a) as a function of the conductor diameter d_w at a constant separation $s_w = 0.7$ mm of the windings; (b) as a function of the winding separation s_w for a constant conductor diameter $d_w = 4.9$ mm. The number of turns was adjusted to keep the inner and outer radii constant at $R_{i,1} = R_{i,2} = 10$ mm, $R_{a,1} = 105$ mm, and $R_{a,2} = 82$ mm.

receiver coil radius of $R_{a,2} = 100$ mm and $N_1 = N_2 = 15$ with $d_w = 4.9$ mm, $s_w = 1$ mm. As indicated in the figure, the maximum of the magnetic coupling for a given air gap tends to larger values of $R_{a,1} > R_{a,2}$. For larger air gaps, the effect is stronger.

It can be shown that for a fixed size of the receiver the mutual inductance L_h exhibits a maximum value at a certain transmitter radius, that is larger than the receiver radius. This explains why also the magnetic coupling shows a maximum at a larger transmitter than receiver coil radius.

F. Quality Factor

The above calculations show, that neither the conductor diameter, nor the winding separation, nor the number of turns have an influence on the magnetic coupling. This allows the conclusion, that the determining factor for the magnetic coupling is the area covered by the winding, as indicated in Fig. 7. Even though this analysis only covered a circular spiral coil, similar results are also expected for rectangular or square coil shapes.

However, the placement of the windings and the absolute length l_w of the litz wire also influence the inductance and the resistance of the coil, which define the inductor quality factor. Fig. 10(a) and (b) show simulation results for the inductor quality factor Q as a function of the conductor diameter d_w and the winding separation s_w respectively. In the simulations, the number of turns was adjusted to keep the inner and the outer coil radius constant. Thus, the number of turns increases with $N \propto 1/d_w$ if the conductor diameter is set to smaller

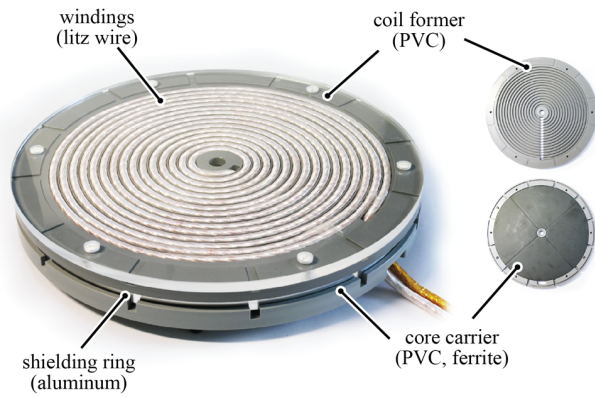


Fig. 11. Photograph of one of the prototype IPT coils used in the experiments.

TABLE II
DATA OF THE EXPERIMENTAL PROTOTYPE

Variable	Min. Value	Max. Value
Outer radius	15.9 mm	105 mm
Inner radius	10 mm	99.1 mm
Number of turns	1	15
Variable	Value	
Litz wire	350 x 0.2 mm	
Ferrite radius	105 mm	
Ferrite thickness	3.75 mm	
Relative permeability	2000	

values and it decreases if the winding separation is chosen larger. It can be seen in Fig. 10(a) that an increasing conductor diameter leads to an improvement of the quality factor $Q \approx \omega_0 L/R$ approximately with $Q \propto d_w$. If ac effects are neglected the winding resistance is reduced with $R \propto l_w/d_w^2 \propto N^3$ and the inductance with $L \propto N^2$ if a larger conductor diameter and a smaller number of turns is used. Hence, increasing the number of turns by using a thinner conductor leads to a reduction of the quality factor with $Q \propto 1/N$.

Fig. 10(b) shows that a reduction of the winding separation s_w with an increasing number of turns leads to an increasing quality factor. This is because the conductor diameter d_w is kept constant, therefore, the resistance $R \propto N$ is increased less than the inductance. Thus, increasing the number of turns by placing more windings of the same conductor on the coil area leads to a higher quality factor. This confirms that a spiral coil should have a small inner radius.

G. Discussion

Because the number of turns, the conductor diameter, and the separation of the windings have no influence on the magnetic coupling k , these relations can be used to optimize the quality factor. The best option for a maximization of the $FOM = kQ$ is to fully utilize the available area by keeping its outer shape, and to fill the coil area with closely spaced windings of a large diameter. However, note that a small separation of the windings also increases the parasitic capacitance and lowers the self-resonance frequency of the coils, which presents an upper limit for the operating frequency.

V. USE OF CORE MATERIALS

In order to improve the magnetic coupling of the inductor further, core materials can be used to guide the flux. They also help reducing the leakage flux. If the available space for the coils is small, as for instance those in biomedical applications, the addition of core material also offers the possibility to produce a higher inductance in

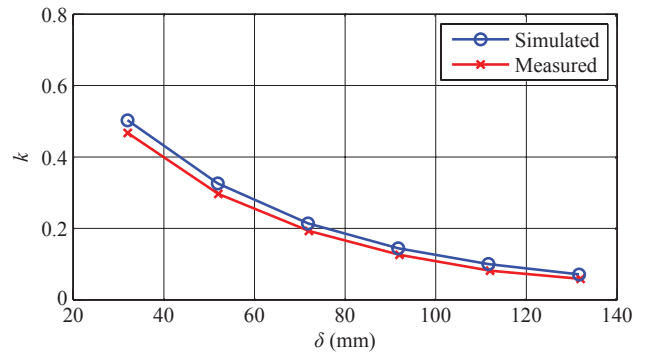


Fig. 12. Comparison between simulated and measured magnetic coupling k of the experimental prototype for different values of the air gap δ .

a given space. This can be required for the impedance matching with respect to the load [22]. Among the potential core materials, ferrite is the most promising option due to its high relative permeability and the low losses at high frequencies, which is required to limit the reduction of the quality factor that results from the core losses. The lower saturation flux density of this material can be tolerated, because the flux is distributed over a relatively large core volume.

For the designs investigated in this paper, mainly two core arrangements are possible: either a ferrite plane can be placed below the windings or a structure similar to a pot-core could be built. With a pot-core, the additional core material in the center of the coil and around the outer radius of the windings would lead to the best performance. A pot-core, however, leads to an increased inductor size. Additionally, for a larger inductor, as would be required for an EV/HEV application, a pot-core has some disadvantages. A ferrite structure of a large size would be fragile and add significant weight to the coil. Moreover, it would need to be custom-made due to the limited availability of large ferrite structures, which would increase the manufacturing cost of inductor. Therefore, most solutions for larger IPT coils found in literature use a ferrite plane built from angular core segments or distributed I-cores as in [10]. This is also typically used in the related induction cooking applications [16]–[18].

VI. MEASUREMENT RESULTS

Based on the results of the presented analysis, an experimental prototype system was constructed. Fig. 11 shows a photograph of one of the designed IPT coils. The coils are constructed from a 350 strand litz wire with a strand diameter of 0.2 mm. The outer diameter of the wire, including the insulation, is 5.2 mm and the windings are separated by 0.7 mm. A coil former made from PVC was designed with an outlet at every turn. In this way, the number of turns as well as the inner and the outer coil diameters can be adjusted. Four 90° ferrite core segments are placed in a compartment below the windings. An aluminum shielding ring can be added at the outer radius of the coil to reduce the leakage flux. Table II contains the geometry data of the prototype.

In order to verify the results of the FE analysis, the prototype transmitter coil was wound with 15 turns. Therefore, its outer radius was $R_{a,1} = 105$ mm and the inner radius was $R_{i,1} = 10$ mm. The receiver had only 7 turns at an outer radius radius of $R_{a,2} = 82$ mm and an inner radius of $R_{i,2} = 41$ mm. The primary coil was fed with a sinusoidal current with a peak value of 20 A and the induced voltage was measured at the open terminals of the secondary while the air gap was increased from 32 mm to 132 mm. The measured coupling coefficients together with the results of the FE simulation are shown

in Fig. 12. The measured values and the simulation results are in good agreement. The small deviation of the simulated values is presumably caused by the (low) conductivity of the ferrite material, which was assumed to be zero for the simulation. Note that for small air gaps, there is a slight increase of the self-inductances of the coils caused by the close proximity of the core of the opposite coil. Therefore, the self-inductances were re-measured for every air gap and the corrected values were included in the results shown in Fig. 12.

VII. CONCLUSION & FUTURE WORK

In this paper it was shown that the magnetic design is crucial for a high transmission efficiency of IPT systems of all power levels. It was shown that for a maximization of the inductor quality factor and the transmission efficiency, the operating frequency can be increased in order to reduce the magnetizing current. This leads to an efficiency improvement as long as the magnetizing current dominates the losses. At the frequency, where the active currents dominate the losses, an optimal transmission frequency exists for a maximum transmission efficiency. However, in a practical system the losses in the power electronics of the supply are likely to limit the operating frequency to lower values. This trade-off will be analyzed in a future work.

It was shown that for a maximization of the magnetic coupling, the enclosed area of the coils is the most important parameter. A comparison of circular, square, and rectangular inductor showed that the exact shape of the coil has only a minor influence. A more detailed comparison of the robustness to misalignment and the leakage flux emissions of these designs will be part of the future work.

It was shown for a circular spiral coil that the design parameters conductor diameter, winding separation, and the number of turns only have a small influence on the magnetic coupling and that the area covered by the winding is the most important factor. However, the inductor quality factor can be improved with an optimized placement of the windings. This can be used to optimize the $FOM = kQ$, for instance if the operating frequency is limited to low values.

An experimental prototype was built to verify the results of the used FE simulations. A measurement of the magnetic coupling showed that the simulations used in this paper are accurate within less than a few percent.

ACKNOWLEDGMENT

The authors would like to thank ABB Switzerland Ltd. for their funding and for their support regarding many aspects of this research project. Additionally, the authors would like to thank E. Waffenschmidt for the fruitful discussions that lead to this publication.

REFERENCES

- [1] C. M. Zierhofer and E. S. Hochmair, "Geometric approach for coupling enhancement of magnetically coupled coils," *IEEE Trans. on Biomedical Engineering*, vol. 43, no. 7, pp. 708–714, 1996.
- [2] M. Ghovanloo and S. Atluri, "A wide-band power-efficient inductive wireless link for implantable microelectronic devices using multiple carriers," *IEEE Trans. on Circuits and Systems*, vol. 54, no. 10, pp. 2211–2221, 2007.
- [3] R. R. Harrison, "Designing efficient inductive power links for implantable devices," in *Proc. of the IEEE International Symposium on Circuits and Systems (ISCAS)*, 2007, pp. 2080–2083.
- [4] K. M. Silay, C. Dehollain, and M. Declercq, "Inductive power link for a wireless cortical implant with biocompatible packaging," in *Proc. of the IEEE Sensors Conference*, 2010, pp. 94–98.
- [5] J. C. Schuder, "Powering an artificial heart: birth of the inductively coupled-radio frequency system in 1960," *Artificial Organs*, vol. 26, no. 11, pp. 909–915, 2002.
- [6] J. C. Schuder, J. H. Gold, and H. E. Stephenson, "An inductively coupled rf system for the transmission of 1 kW of power through the skin," *IEEE Trans. on Biomedical Engineering*, vol. 18, no. 4, pp. 265–273, 1971.
- [7] C. Reinhold, P. Scholz, W. John, and U. Hilleringmann, "Efficient antenna design of inductive coupled RFID-systems with high power demand," *Journal of Communications*, vol. 2, no. 6, pp. 14–23, 2007.
- [8] K. Finkensteller, *RFID-Handbook: Fundamentals and Applications in Contactless Smart Cards, Radio Frequency Identification and Near-Field Communication*, 3rd ed. John Wiley & Sons, 2010.
- [9] E. Waffenschmidt and T. Staring, "Limitation of inductive power transfer for consumer applications," in *Proc. of the 13th European Conference on Power Electronics and Applications (EPE)*, 2009, pp. 1–10.
- [10] M. Budhia, G. A. Covic, and J. T. Boys, "Design and optimization of circular magnetic structures for lumped inductive power transfer systems," *IEEE Trans. on Power Electronics*, vol. 26, no. 11, pp. 3096–3108, 2011.
- [11] M. Budhia, J. Boys, G. Covic, and C. Huang, "Development of a single-sided flux magnetic coupler for electric vehicle IPT charging systems," *IEEE Trans. on Industrial Electronics*, vol. 60, no. 1, pp. 318–328, 2013.
- [12] J. Huh, S. W. Lee, W. Y. Lee, G. H. Cho, and C. T. Rim, "Narrow-width inductive power transfer system for online electrical vehicles," *IEEE Trans. on Power Electronics*, vol. 26, no. 12, pp. 3666–3679, 2011.
- [13] R. Bosshard, J. Mühlethaler, J. W. Kolar, and I. Stevanović, "The η - α -Pareto front of inductive power transfer coils," in *Proc. of the 38th IEEE Industrial Electronics Conference (IECON)*, 2012.
- [14] R. Bosshard, U. Badstübner, J. W. Kolar, and I. Stevanović, "Comparative evaluation of control methods for inductive power transfer," in *Proc. of the 1st International Conference on Renewable Energy Research and Applications (ICRERA)*, 2012.
- [15] D. Kürschner, "Methodischer Entwurf toleranzbehalteter induktiver Energieübertragungssysteme," Ph.D. dissertation, Otto-von-Guericke University, Magdeburg, 2009.
- [16] M. Kamil, S. Yamamoto, and M. Abe, "A 50-150 kHz half-bridge inverter for induction heating applications," *IEEE Trans. on Industrial Electronics*, vol. 43, no. 1, pp. 163–172, 1996.
- [17] O. Lucía, L. A. Barragán, J. M. Burdío, O. Jiménez, and D. Navarro, "A versatile power electronics test-bench architecture applied to domestic induction heating," *IEEE Trans. on Industrial Electronics*, vol. 58, no. 3, pp. 998–1007, 2011.
- [18] J. Acero, J. M. Burdío, L. A. Barragán, D. Navarro, R. Alonso, J. R. García, F. Monterde, P. Hernández, S. Llorente, and I. Garde, "The domestic induction heating appliance: An overview of recent research," *Proc. of the 23th IEEE Applied Power Electronics Conference and Exhibition (APEC)*, pp. 651–657, 2008.
- [19] *Guidelines for Limiting Exposure to Time-Varying Electric and Magnetic Fields (1 Hz to 100 kHz)*, International Commission on Non-Ionizing Radiation Protection (ICNIRP) Std., 2010.
- [20] *Guidelines for Limiting Exposure to Time-Varying Electric, Magnetic and Electromagnetic Fields (up to 300 GHz)*, International Commission on Non-Ionizing Radiation Protection (ICNIRP) Std., 1998.
- [21] G. Vandevoorde and R. Puers, "Wireless energy transfer for stand-alone systems: A comparison between low and high power applicability," *Sensors A*, vol. 92, no. 1-3, pp. 305–311, 2000.
- [22] K. Van Schuylenbergh and R. Puers, *Inductive Powering: Basic Theory and Application to Biomedical Systems*, 1st ed. Springer Science, 2009.
- [23] R. W. Erickson and D. Maksimovic, *Fundamentals of Power Electronics*, 2nd ed. Springer Science, 2001.
- [24] J. Mühlethaler, "Modeling and multi-objective optimization of inductive power components," Ph.D. dissertation, Swiss Federal Institute of Technology Zurich (ETHZ), 2012.
- [25] S.-H. Lee and R. D. Lorenz, "A design methodology for multi-kW, large airgap, MHz frequency, wireless power transfer systems," *Proc. of the IEEE Energy Conversion Congress and Exposition (ECCE)*, pp. 3503 – 3510, 2011.
- [26] A. Kurs, A. Karalis, R. Moffatt, J. D. Joannopoulos, P. Fisher, and M. Soljacic, "Wireless power transfer via strongly coupled magnetic resonances," *Science*, vol. 1143254, pp. 83–86, 2007.
- [27] G. Ortiz, D. Bortis, J. W. Kolar, and O. Apeldoorn, "Soft-switching techniques for medium-voltage isolated bidirectional DC/DC converters in solid state transformers," in *Proc. of the 38th IEEE Industrial Electronics Conference (IECON)*, 2012.
- [28] S. I. Babic and C. Akyel, "Calculating mutual inductance between circular coils with inclined axes in air," *IEEE Trans. on Magnetics*, vol. 44, no. 7, pp. 1743–1750, 2008.